Solid Freeform Fabrication 2023: Proceedings of the 34th Annual International Solid Freeform Fabrication Symposium – An Additive Manufacturing Conference
Reviewed Paper

Investigation of the influence of process parameters on productivity in the LPBF process for the material Inconel 718

C. Bödger[1,2], S. Gnaase[1], D. Lehnert[1,2] and T. Tröster[1]

[1]Automotive Lightweight Design (LiA), Paderborn University, D-33098 Paderborn
[2]Direct Manufacturing Research Center (DMRC), Paderborn University, D-33100 Paderborn

Abstract

The nickel-based alloy Inconel 718, which is used in aerospace technology, poses a great challenge to conventional machining due to its high strain hardening and toughness. Here, the laser powder bed fusion process (LPBF) offers an alternative with potential savings if sufficiently high productivity can be achieved. Based on the parameter study carried out, starting from the SLM Solutions standard parameters for the manufacturing of components, exposure parameters could be developed to realize manufacturing with 120 µm and 150 µm layer thickness, with almost the same geometric accuracy. For this purpose, the process parameters of laser power, focus diameter, hatch distance and scan speed were varied. The negative defocusing of the laser showed a positive effect on the density of the parts, realizing densities ≥ 99.94 %, with high dimensional stability and good mechanical properties. Considering the reduced manufacturing time of up to 61 %, a significant increase in productivity was achieved.

Introduction

Additive manufacturing processes offer great potential for lightweight construction applications. In the LPBF process, components are manufactured layer by layer, which in contrast to metal-cutting manufacturing processes, allows great freedom of design, up to 90 % less material waste in some cases and low material wear of (post) processing tools. The material savings alone are linked to a correspondingly reduced energy input for material production and processing. A current limitation of the LPBF process is its low productivity compared to conventional manufacturing [1].

Higher productivity may lead to a wider field of application and thus to realization of material and energy savings through use of recycled powder. In previous research, an approach to increase productivity has already been successfully validated by increasing the layer thickness in the LPBF process from 60 µm to 180 µm [2]. This approach is extended in the present work by enlarging the laser focus. By widening the laser focus, a larger powder bed area can be exposed per scan vector and the distance between the scan vectors can be increased. This can result in a 50 % savings in exposure time, further increasing productivity. First promising findings on the influence of focus widening have already been obtained in previous work. The new approach was validated using the nickel-based alloy 718. Due to its high strain hardening and toughness, conventional machining presents a challenge due to high tool wear and low material removal rates [3-5]. LPBF can be an alternative with significant savings potential if sufficiently high productivity is achieved. As a result, the part can be built with minimal positive offset to enable the application of post processing by conventional machining while minimizing the amount of material which must be removed. This leads to cost and time savings in machining.

Experimental details

All samples were produced with an SLM 280 2.0 (SLM Solutions Group AG). The machine has a build envelope of (L x W x H) 280 x 280 x 365 mm³. A 700 W ytterbium fiber laser is installed in the optical unit. A rubber lip was used for the coater and the powder deposition was bi-directional. For each build job, the preheat temperature was set to 200 °C and a steel platform was used. The manufacturing was done under Argon 4.6 inert gas atmosphere.

The nickel-based alloy Inconel 718 from m4p was used as the powder material. The chemical composition of the material according to ASTM B637 can be found in Table 1. The virgin powder was spherical with particle size distribution ranging from 10 - 45 µm. The used powder was sieved with a mesh size of 65 µm and vacuum dried (residual moisture < 5 %) before the LPBF process to avoid a negative influence on the build process due to excess moisture or enlarged particles.

Fe	Ni	Cr	Ta+Nb	Mo	Ti	Co	Al	Si	Mn	Cu	C	P	S	B
Bal.	50.0-55.0	17.0-21.0	4.75-5.5	2.8-3.3	0.65-1.15	0-1.0	0.2-0.8	0-0.35	0-0.35	0-0.3	0-0.08	0-0.015	0-0.015	0-0.006

Table 1: Chemical composition of Inconel 718 (wt. %).

Results and Discussion

Parameter development:

To determine a LPBF parameter set with the target of highly dense samples and increased build rate, a Central Composite Design (CCD) type DoE was chosen as the design strategy. The parameters laser power, scan speed, and hatch distance were varied at layer thicknesses of 120 µm, 150 µm, and 180 µm according to Table 2 and the contour parameter was disabled.

Parameter	Value range	Step width
Laser power [W]	460 - 640	45
Scanning speed [mm/s]	500 - 900	100
Hatch distance [mm]	0.16 - 0.2	0.01
Focus diameter [µm]	80 - 160	11

Table 2: Investigated parameter combinations per layer.

The laser focus was initially kept constant at 113 µm. This value was taken from SLM Solutions standard parameter set for Inconel 718. As a result, 35 cubic specimens with a geometry of 10 x 10 x 10 mm³ were produced for each layer thickness in one build job and at a 45° angle to the gas flow direction (see Figure 1).

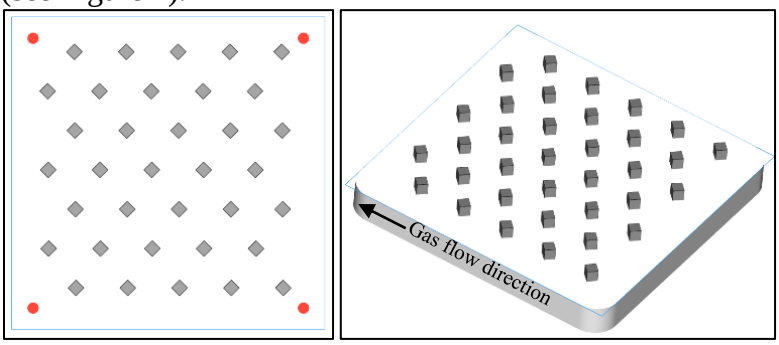

Figure 1: Distribution and alignment of the cubes on the building platform.

Table 3 shows an overview of the parameters with the highest relative density of the respective layer thickness compared to the 60 µm standard layer thickness. In addition, the volumetric energy density and build rate per layer thickness are compared. To determine the density of the samples, contrast images of each fabricated cube were taken in the xz-plane using a Keyence VHX-5000 and analyzed using the program ImageJ.

Layer thickness	Hatch distance [µm]	Laser power [W]	Scanning speed [mm/s]	Volumetric energy density [J/mm^3]	Relative density [%]	Build-up rate [cm^3/h]
60 µm	140	350	887	46.97	>99.50	26.82
120 µm	160	550	900	31.83	99.92	62.20
150 µm	160	550	900	25.46	99.90	77.76
180 µm	160	460	700	22.82	99.84	72.58

Table 3: Parameter with the highest relative density compared to the standard parameter.

Subsequently, using the parameters that resulted in the highest relative density, further cube samples were fabricated, each with three replicate tests to investigate the relative density. In this step, only the focus diameter was varied from 80 - 160 µm for each layer thickness.
The focus diameter $Ø_f$ is the diameter of the laser spot projected onto the surface of the powder. This increases with increasing focus shift Δz. The focus shift (also called defocus) is a measure of the offset of the laser focus from the build surface. Figure 2 shows this relationship schematically. Also shown is the beam path of the laser beam. Under negative defocus, the laser beam divergently hits the build surface, while under positive defocus, the laser beam converges [6]. The minimum beam diameter and Rayleigh length are machine dependent and must be determined in a beam acoustics measurement. Table 4 shows the focus diameters depending on the focus shift. It is important to differentiate between focus shift Δz and focus diameter $Ø_f$. The focus shift Δz is the adjustable parameter of the system, the focus diameter is the resulting influence on the build process and the component.

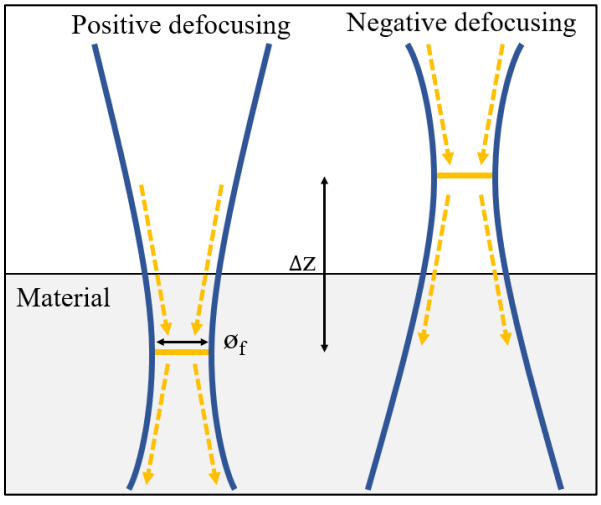

Figure 2: Schematic representation of positive and negative defocusing.

Focus shift Δz [mm]	Focus diameter $Ø_f$ [µm]
-1 / 1	79
-2 / 2	87
-3 / 3	99
-4 / 4	113
-5 / 5	130
-6 / 6	147
-7 / 7	165

Table 4: Focus diameter øf as a dependence of the focus shift Δz.

In the following preliminary investigations, the influence of the positive and negative focus shift Δz was investigated. For this purpose, all other parameter settings were kept constant except for the focus shift. The micrographs for Δz = ±3 (see Figure 3a and 3b) show by comparison that the relative density is significantly higher in the direction of negative defocusing. With positive defocus, the relative density decreases due to keyhole defects and gas porosity. With the same settings, this problem is significantly reduced for negative defocus. The graph (see Figure 3c) reflects what could be seen in the micrograph. With a negative focus shift Δz, the process resembles heat conduction welding (heat conduction mode) due to divergent beam path, despite high energy densities, characterized by a low melt pool depth and high width of the melt pool [7]. Positive defocusing favors deep welding, and keyhole defects and gas inclusions are increasingly formed as the powder evaporates [8]. Overall, heat conduction welding is preferred in the SLM process. In the preliminary tests, the average relative density value in the negative focus direction is always above the target value of 99.9 %. Therefore, only the negative focus shift was considered in the further course of the project.

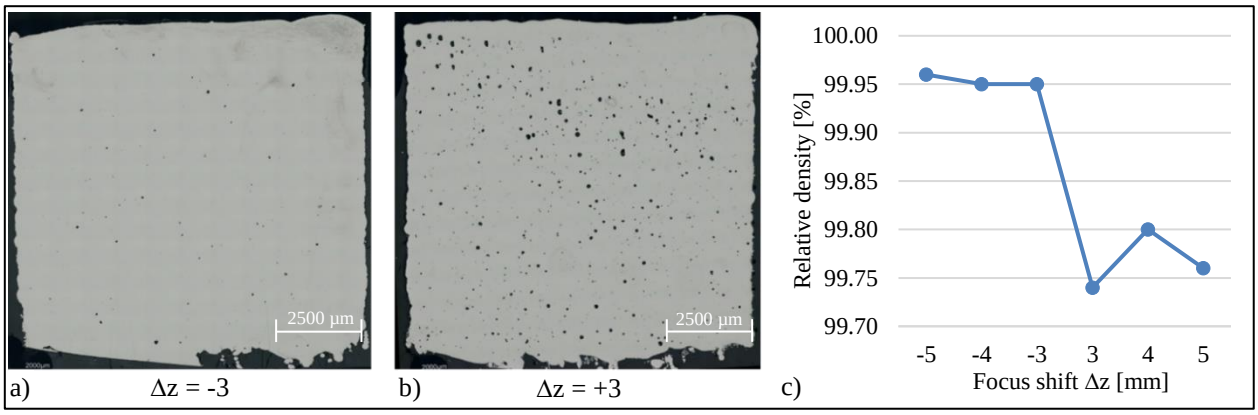

Figure 3:Comparison of same parameter settings with negative (a) and positive (b) focus shift Δz. Relative density as a function of the focus shift Δz (c).

The influence on the relative density is shown in Figure 4. Regardless of the layer thickness, the increase in focus diameter has a significant/positive influence on the relative density of the samples. Relative densities of 99.92 % (120 µm layer thickness), 99.90 % (150 µm layer thickness) and 99.84 % (180 µm layer thickness) were achieved with the standard focus diameter of 113 µm. Reducing the diameter to 80 µm resulted in lower relative densities, while increasing the focal diameter to 165 µm resulted in an increase in the respective relative densities: 99.95 % (120 µm layer thickness), 99.94 % (150 µm layer thickness), 99.94 % (180 µm layer thickness).

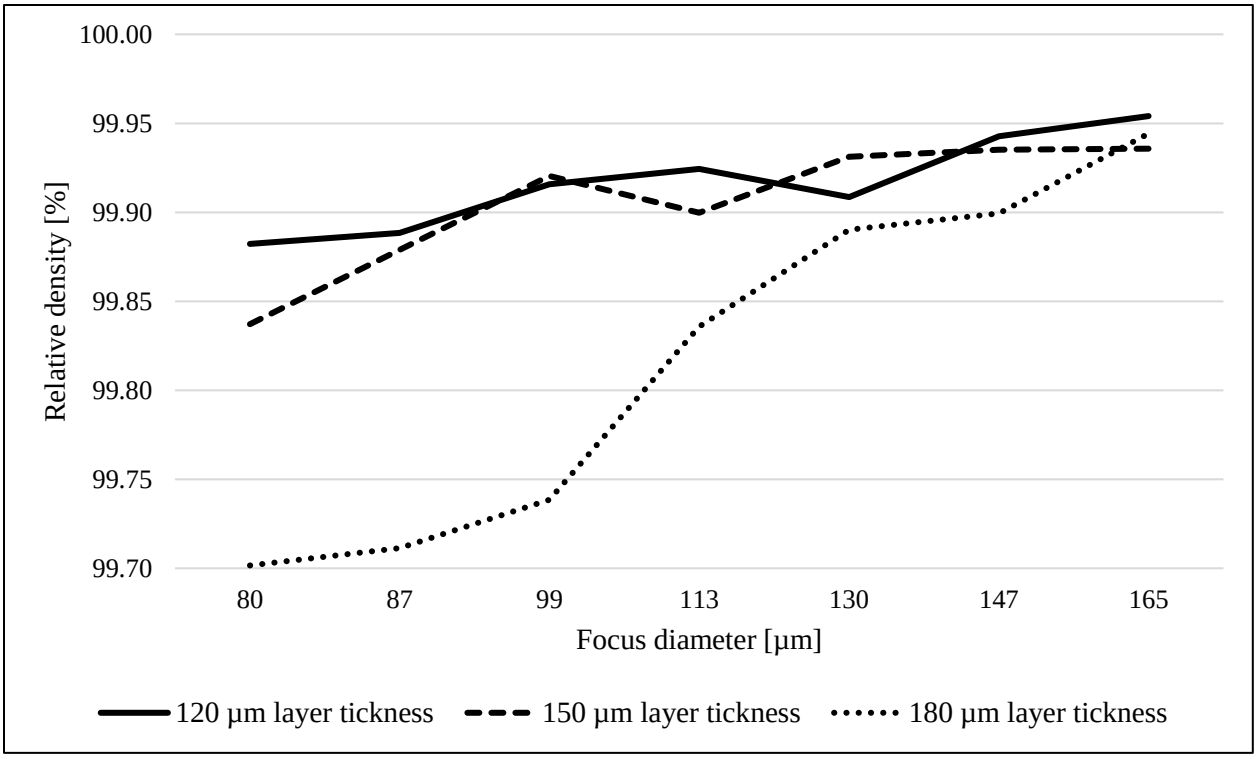

Figure 4: Influence of the focus diameter on the relative density.

Figure 5 shows the micrographs of the parameter combinations with the highest relative density per layer thickness. The grid-like representation of the micrographs is due to the microscope's acquisition mode. The defects at the bottom of each image are due to poor heat dissipation because of the block support structure used and were not considered in the density determination. Block supports consist of a grid of lines, where each line usually assumes the thickness of the melt pool. The relative density was measured along the contour, as exemplified for the 120 µm layer thickness shown in blue. In addition, the images show minimal gas porosity across the entire geometry. The performance parameter combination for the respective layer thickness were used to determine the mechanical properties.

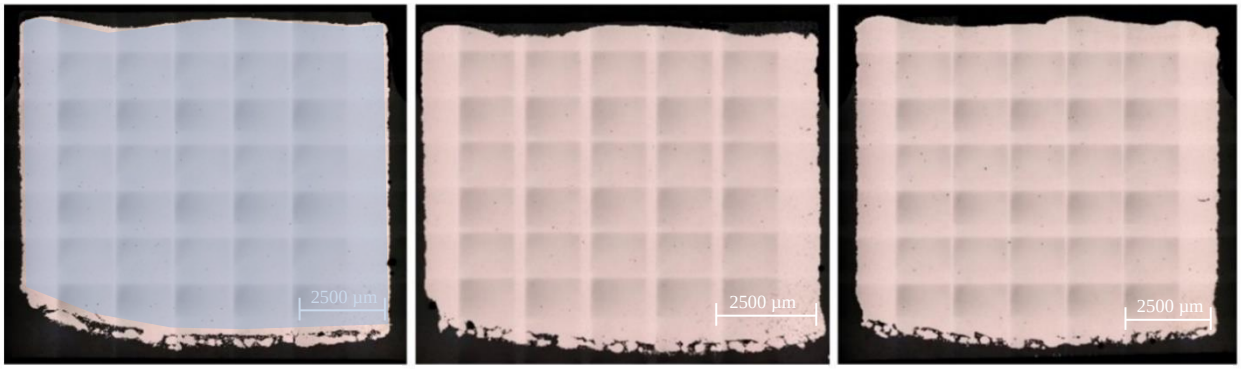

Figure 5: Micrographs of the parameter combinations with the highest relative density per layer thickness.

Determination of the mechanical parameters:

A mechanical characterization of the processed material was carried out by means of tensile tests on round tensile specimens according to DIN 50125:2004-1 Form A and Charpy impact tests (DIN EN ISO 148-1:2017:5). For this purpose, ten cylinders (Ø 10 mm) with a height of 99 mm and five cuboid specimen with dimensions of 55 x 10 x 10 mm³ were initially manufactured for each layer thickness. Due to the previously recognized negative influence of the support structure on the geometry, the further specimens were built directly onto the building platform to achieve better heat dissipation.

Tensile tests: After manufacturing the cylinders for the tensile tests were conventionally turned to the dimensions according to the mentioned standard. The tensile tests were carried out using a ZwickRoell HB 250 machine in accordance with DIN EN ISO 6892. The round specimens were tested using a continuous displacement (v = 4 mm/min). The strain in the test area was recorded with a contact extensometer. The measured results for Young's modulus, yield strength, tensile strength, and elongation at break of the additively processed Inconel 718 samples are listed in Table 5. Compared to the 60 µm standard parameter, doubling the layer thickness to 120 µm resulted in a higher Young's modulus (185 GPa) with almost the same elongation at break (approx. 31 %) and a slightly increased tensile strength with 942 MPa [6]. Only the yield strength of 590 MPa was below the reference value from the datasheet of 606 MPa. The tensile specimens produced with 150 µm layer thickness gave a modulus of elasticity of around 188 GPa. The average tensile strength was 928 MPa. This corresponds to a deviation of -1.5 % compared with the data in the manufacturer's data sheet. The fracture failure of the specimens occurs on average at an elongation of 25 % and thus deviates by -7 % from the reference value. The 180 µm parameters led to an increase in the Young's modulus to 185 GPa. However, the yield strength was reduced to 557 MPa and the tensile strength to 778 MPa. For the elongation at break, the average value was 9 %.

60 µm (Standard)	Young´s Modul [GPa]	Yield Strength [MPa]	Tensile Strength [MPa]	Elongation at break [%]
Mean:	154	606	942	31
Standard deviation:	13	8	15	5
120 µm				
Mean:	185	590	955	30
Standard deviation:	8	16	14	3
150 µm				
Mean:	188	571	928	25
Standard deviation:	7	14	24	6
180 µm				
Mean:	185	557	778	9
Standard deviation:	13	33	46	3

Table 5: Determined mechanical properties of the tensile tests per layer thickness.

Selected stress-strain curves reflecting the mean results of the samples manufactured with the respective layer thicknesses are shown in Figure 6. Using the 120 µm parameter set, slightly higher stresses could be realized with a minimal lower strain of -1 %. Even with a layer thickness of 150 µm, a progression of the stress-strain curve can be seen which is almost identical to the one of 60 µm samples. However, in this case the elongation is reduced by 5 %. The parameter for 180 µm, on the other hand, shows a significantly reduced elongation at lower stress.

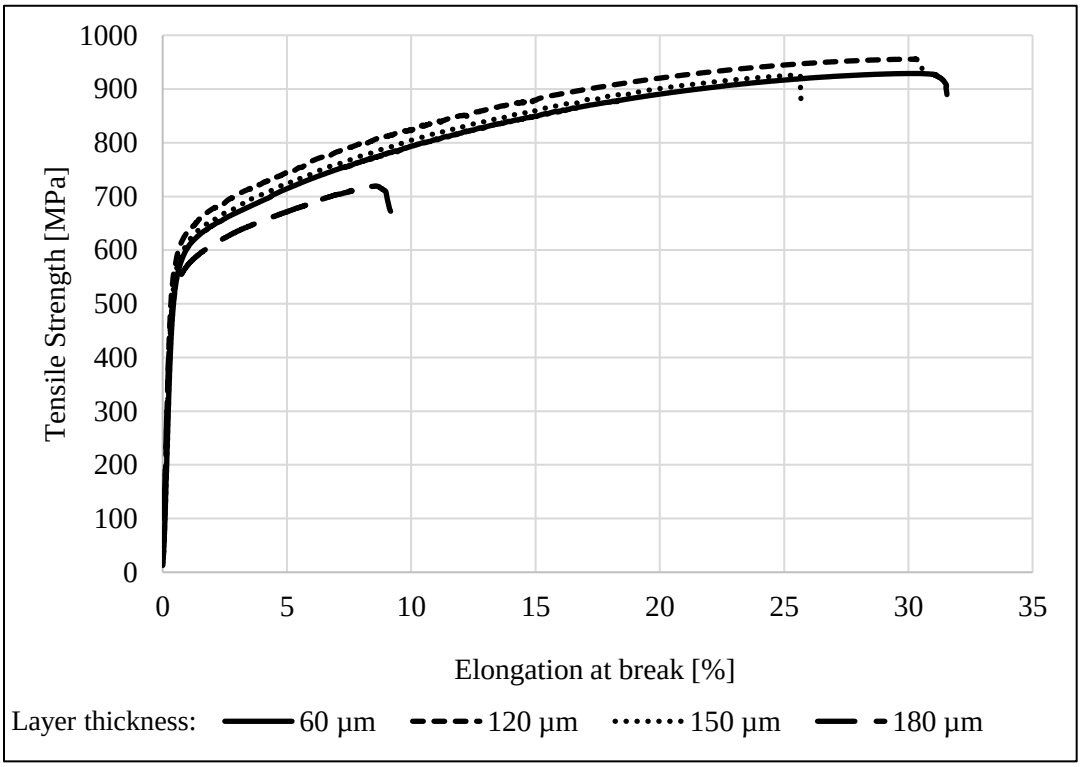

Figure 6: Selected stress-strain curves from tensile tests of Inconel 718.

Charpy impact tests: The Charpy impact test offers the possibility of investigating the brittle fracture tendency of a material. A notched specimen is smashed with a pendulum hammer and the impact energy consumed is measured. In this case a V-notch had to be eroded into each of the components. A 300 J test hammer was used to perform the test. Figure 7 shows that the parameter with 120 µm layer thickness has the highest impact strength ($\bar{x}$ = 91 J). This value exceeds the reference value of the powder manufacturer (80 J) by approx. 14 % [6]. The impact strength of the 150 µm layer thickness exhibits an average value of 80 J. Only the layer thickness of 180 µm ($\bar{x}$ = 65.8 J) showed a significantly lower notched impact strength. A reason for the earlier failure may be the distribution of the pores. The specimens for 120 µm and 150 µm showed a homogeneous distribution of small gas pores in the normal range. The specimen for 180 µm layer thickness showed a lower gas porosity, but the few pores found were significantly larger in comparison. Larger local pores can lead to faster material failure than small and homogeneously distributed pores in the component.

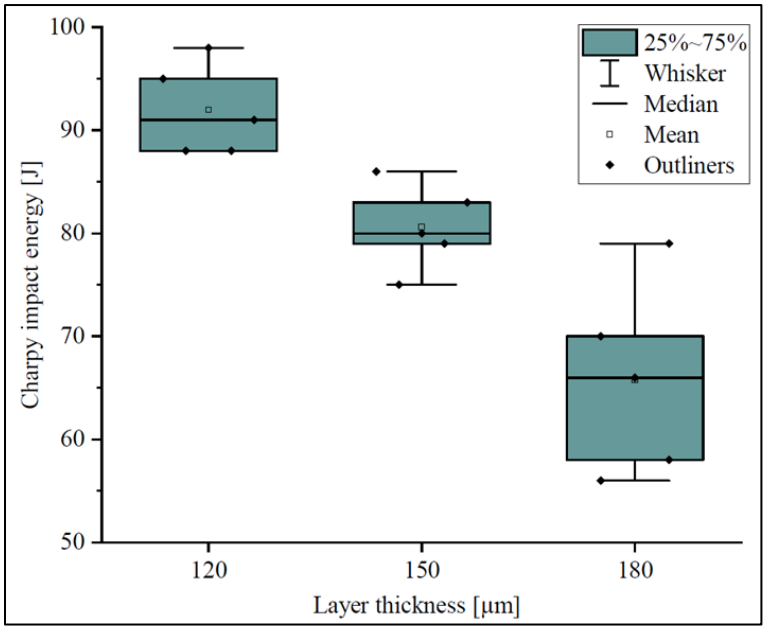

Figure 7: Results of the Charpy impact tests per layer thickness.

Design and manufacture demonstrator component:

The parameter sets for 120 µm and 150 µm layer thickness were finally checked with regards to their transferability to other geometries. For this purpose, a test specimen construction job was created according to DIN EN ISO/ASTM 52902. This contains linear artefacts, circular artefacts, resolution pin artefacts, resolution slot artefacts, resolution hole artefacts, resolution rib artefacts and a test artefact for surface finish. Figure 8 shows the individual test specimens arranged on the build platform. The measurements were performed manually with a digital caliper. Therefore, a tolerance limit of ± 0.1 mm to the nominal value was set. Due to the unsatisfactory mechanical properties, no demonstrator was manufactured for 180 µm layer thickness.

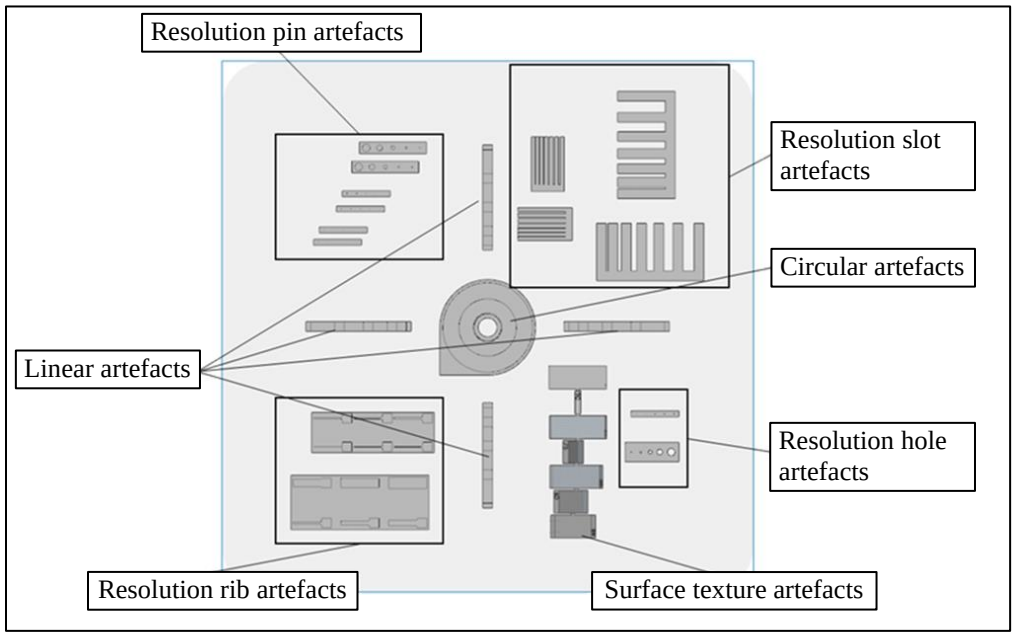

Figure 8: Demonstrator build job for validation according to DIN EN ISO/ASTM 52902.

The linear test artefacts each consist of three cubes with an edge length of 5 mm and projections of 2.5 mm at the ends. Two test specimens were tested along the coating direction and two test specimens were tested transverse to the coating direction. No significant difference was found between the orientations for either layer thickness. The evaluated sizes of the circular test artefacts had diameters between 14 and 50 mm. For both coating thicknesses, each diameter deviated into the negative. In particular, the outer diameter of the inner ring deviated by -1.1 mm (-7 %) from the nominal value of 16 mm for both layer thicknesses. With both layer thicknesses, resolution pins could only be produced with a minimum diameter of 0.2 mm. It should be emphasized that for both layer thicknesses, the pins from 0.4 mm diameter were manufactured with minimal to no deviation. Resolution holes ≤ 1 mm were present at both layer thicknesses but could not be measured with the available measuring equipment. The resolution hole artefacts with a diameter of 2 - 4 mm all deviated by -0.1 mm from the nominal value. Test walls with a nominal thickness of 0.2 mm and less were printed with a thickness of 0.3 - 0.4 mm, regardless of the layer thickness, and were thus practically not manufacturable. From a thickness of 0.4 mm, only minimal differences from the nominal value were measurable. The test specimen for resolution slot artefacts was again built in two directions to the coating. Regardless of layer thickness and orientation, slots with a size of 0.1 and 0.2 mm were visible but not measurable. Resolution slots ≥ 0.4 mm were made true to size.
Overall, no significant differences in dimensional accuracy were observed between the 120 µm and 150 µm layer thicknesses. However, the lower limits of manufacturability for wall thicknesses, resolution pins, holes and slots were evident and must be considered for manufacturing.
The surface finishes depending on the component angle can be taken from Table 6 and compared with the values for 60 µm layer thickness (0°: Ra = 8 and Rz = 50) [9]. Regardless of the angle, it could be seen that the roughness values increase with increasing layer thickness and the reference values of the standard parameter were not reached. The highest roughness values were caused by a 15° angle. Based on the low surface finish, reworking of the components must be considered.

Layer thickness		0°	15°	30°	45°	60°	75°	90°
120	R_a	8.7	24.5	16.8	15.3	11.7	7.3	8.3
	R_z	81.7	152.1	114.5	114.1	84.1	53.2	53.4
150	R_a	9.7	32.1	22.4	19.0	15.8	9.0	9.0
	R_z	69.6	188.1	161.0	133.6	129.4	65.4	65.3

Table 6: Surface roughness of the different layer thicknesses in angular dependence.

Quality and economic considerations

In series production with an increased number of components within a build job, the machine time plays a key role in reducing the cost of the components. A reduction in machining time therefore means a higher economic efficiency of the LPBF process. The machining time consists of the time for production preparation, the actual component production, and the post-processing. In addition, the machining time is divided into the exposure time and the coating time of the individual layers [1]. A higher build-up rate due to changed machine parameters, i.e., scan speed and hatch distance, influences the exposure time of the part and depends on the area to be scanned. A higher layer thickness, in turn, shortens the total powder build-up time, as the number of layers required for a given build height decreases. Accordingly, the machine must apply new powder less frequently.

The comparison of the process build times was carried out using the demonstrator (see Figure 8). The process times for LPBF production of the component were compared for different layer thicknesses (cf. Figure 9). The parameters developed with increased layer thicknesses were compared with the standard parameter for Inconel 718.

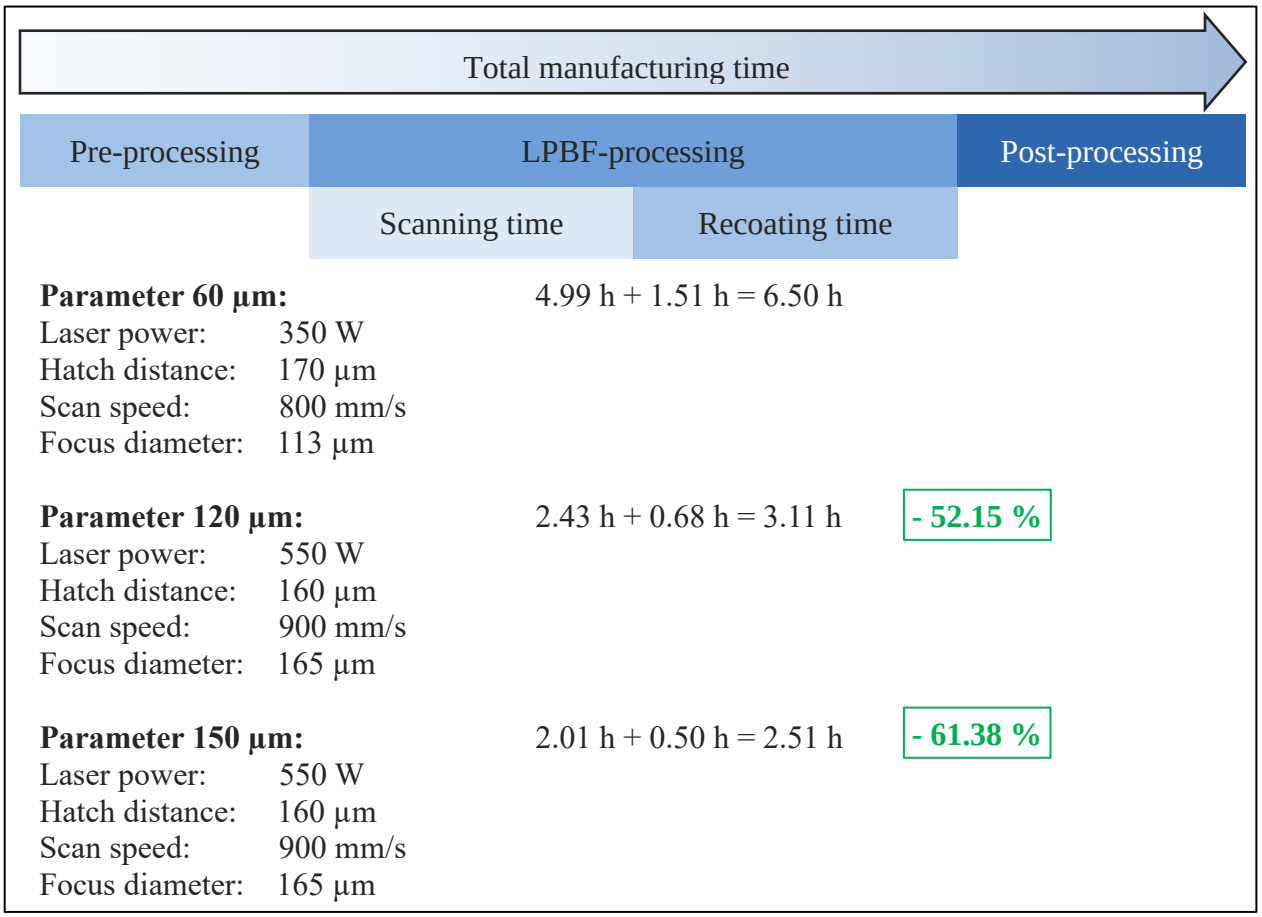

Figure 9: LPBF manufacturing time for different layer thicknesses.

As can be seen from the work carried out in this project, the parameter combination with a layer height of 120 µm and a buildup rate of 62.2 cm³/h resulted in a rate more than twice as high as for the standard parameter (26.82 cm³/h) [9]. However, a calculation of the processing time exclusively via the build-up rate of the parameter leads to inaccurate results since the machine-dependent recoating time is not considered. Therefore, the actual build-up times were taken from the production log of the line. Based on the 120 µm layer thickness, a reduction in production time of 52.15 % was achieved. With a layer thickness of 150 µm, a time reduction of 61.38 % was possible. Compared to conventional production of the demonstrator, the greatest potential lies in the reduced use of materials. In this case, the demonstrator would have to be milled from the solid, which would lead to high tool wear due to the high strength of nickel alloys. In addition, some geometries could not be produced at all due to undercuts. The component volume of the demonstrator is 99.4 cm³. However, conventional production would have required a semi-finished product measuring 28 x 28 x 4.3 cm³ (3,371.2 cm³). Thus, 3,271.8 cm³ or 97.05 % (26.8 kg) of raw materials could be saved by additive manufacturing.

Conclusion

Based on the parameter study carried out, starting from the standard parameters for the manufacture of components made of Inconel 718 with a layer thickness of 60 µm, it was possible to develop exposure parameters to realize a production with a layer thickness of 120 µm and 150 µm. Negative defocusing of the process laser had a positive effect on the density of the components. The mechanical parameters showed only slight reductions compared with the reference value. The reason for this may be the different proportion of the number of pores to the pore size. Larger local pores (180 µm layer thickness) can lead to faster material failure than small and homogeneously distributed pores (120 & 150 µm layer thickness) in the component. Overall, densities $\geq$ 99.94 %, with a high dimensional stability were realized. Considering the reduced production time by 52 % (120 µm) and 61 % (150 µm), a significant increase in productivity was achieved. This favors the further establishment of the technology in existing markets through higher volumes, but also to the expansion of business areas. However, it must be pointed out, that the surface quality decreases with increasing layer thickness and, depending on the application, post processing of the components may be necessary.

The advantages of a nickel alloy, such as high strength, heat and corrosion resistance, can be exploited by means of the LPBF process to produce complex structures. In aerospace engineering, Inconel 718 is one of the most important materials for manufacturing turbine components [10]. In addition, the rapid production of high-strength spare parts offers another field of application for manufacturing using LPBF.

References

[1] Bierdel, M.; Pfaff, A.; Kilchert, S.: Köhler, A.R.; Baron, Y.; Bulach, W.: „Ökologische und ökonomische Bewertung des Ressourcenaufwands Additive Fertigungsverfahren“ (2019)

[2] Ahlers, D.: „Ressourceneffizienz im Laserstrahlschmelzprozess durch Optimierung der Schichtdicke / R-LOS“ (2021), Förderkennzeichen: 005-2005-0004_093, proges.nrw

[3] Pariada, A. K.; Maity, K.: “Comparison the machinability of Inconel 718, Inconel 625 and Monel 400 in hot turning operation.” In: Engineering Science and Technology, an International Journal 21 (2018), no. 3, pp. 364-370

[4] Xavior, M. A.; Patil, M.; Maiti, A.; Raj, M.; Lohia, N.: “Machinability studies on Inconel 718.” In: IOP Conference Series: Materials Science and Engineering 149 (2016)

[5] Rahman, M. ; Seah, W.K.H. ; Teo, T. T.: “The machinability of Inconel 718”. In: Journal of Materials Processing Technology 63 (1997), 1-3, pp. 199-204

[6] Metelkova, J. et al.: “On the influence of laser defocusing in Selective Laser Melting of 316L.” In: Additive Manufacturing 23 (2018), pp. 161–169

[7] Heß, T.: „Beitrag zur Qualifizierung des pulverbettbasierten Laserstrahlschmelzens zur Serienfertigung am Beispiel der Triebwerksindustrie“. Dissertation. Karlsruhe: KIT (2015)

[8] King, W. E.; H. D. Barth; V. M. Castillo; G. F. Gallegos; J. W. Gibbs; D. E. Hahn; C. Kamath; A. M. Rubenchik: „Observation of keyhole-mode laser melting in laser powder-bed fusion additive manufacturing“. Journal of Materials Processing Technology (2014)

[9] SLM Solutions AG: Materialdatenblatt Ni-Alloy IN718 / 2.4668 (2022) https://www.slm-solutions.com/fileadmin/Content/Powder/MDS/MDS_Ni-Alloy_IN718_0719.pdf

[10] Special Metals Corporation: Inconel 718 Datenblatt (2007) https://www.specialmetals.com/documents/technical-bulletins/inconel/inconel-alloy-718.pdf